A Grid Search of Fibrosis Thresholds for Uncertainty Quantification in Atrial Flutter Simulations

Benjamin A Orkild[1,2,3], Jake A Bergquist[1,2,3], Eric N Paccione [1,2,3], Matthias Lange[2], Eugene Kwan[1,2], Bram Hunt[1,2], Rob S MacLeod[1,2,3], Akil Narayan[3], Ravi Ranjan[1,2,4]

[1] University of Utah Department of Biomedical Engineering, Salt Lake City, USA
[2] Nora Eccles Treadwell CVRTI, University of Utah, SLC, UT, USA
[3] Scientific Computing and Imaging Institute, Salt Lake City, USA
[4] School of Medicine, University of Utah, SLC, UT, USA

Abstract

Atypical atrial flutter (AAF) is a cardiac arrhythmia commonly developed following catheter ablation for atrial fibrillation. Patient-specific computational simulations of propagation have shown promise in prospectively predicting AAF reentrant circuits and providing useful insight to guide successful ablation procedures. These patient-specific models require a large number of inputs, each with an unknown amount of uncertainty. Uncertainty quantification (UQ) is a technique to assess how variability in a set of input parameters can affect the output of a model. However, modern UQ techniques, such as polynomial chaos expansion, require a well-defined output to map to the inputs. In this study, we aimed to explore the sensitivity of simulated reentry to the selection of fibrosis threshold in patient-specific AAF models. We utilized the image intensity ratio (IIR) method to set the fibrosis threshold in the LGE-MRI from a single patient with prior ablation. We found that the majority of changes to the duration of reentry occurred within an IIR range of 1.01 *to* 1.39*, and that there was a large amount of variability in the resulting arrhythmia. This study serves as a starting point for future UQ studies to investigate the nonlinear relationship between fibrosis threshold and the resulting arrhythmia in AAF models.*

1. Introduction

Atypical atrial flutter (AAF) is a cardiac arrhythmia commonly developed following catheter ablation for atrial fibrillation [1]. Additional catheter ablation is the most common treatment for AAF; however, up to 63% of patients experience AAF recurrence 1-year post-ablation [2]. There is a critical need to develop more robust and lasting AAF treatment strategies.

Patient-specific computational simulations of propagation have shown promise in prospectively predicting AAF reentrant circuits and providing useful insight to guide successful ablation procedures [3]. However, these simulations require the user to create geometric models from images and select ionic model parameters, both of which introduce sources of uncertainty and error to the resulting AAF. Variability in the ionic model parameters has been shown to affect the reentrant circuits of patient-specific simulations [4]. Variability in the geometric models, which are often based on late gadolinium-enhanced (LGE) MRI images, arises from several user-defined image-intensity thresholds. Specifically, the fibrosis regions are generated based on a choice of threshold, which can be selected based on a variety of methods [5]. The selection of the fibrosis threshold can introduce unknown variability into the generated fibrosis region. This variability has an unknown effect on the output of these patient-specific simulations. In order to use patient-specific models clinically in a safe and effective manner, we must understand the relationship between the variability of the input parameters and the output of the simulation.

Uncertainty quantification (UQ) is a technique to assess how variability in a set of input parameters can affect the output of a model [6]. However, modern UQ techniques, such as polynomial chaos expansion, require a well-defined output to map to the inputs. Clinically, the desired outputs from patient-specific AAF simulations are the locations and characteristics of the AAF circuits. Because subtle changes to the model parameters may result in substantial changes to the AAF reentry circuits, automatically identifying these characteristics from simulation results and formulating them into an interpretable yet comprehensive UQ output is challenging. Initial studies must first explore the broad behavior of such AAF models in the context of input uncertainty to identify a suitable strategy for the application of more advanced UQ techniques.

In this study, we focused on changes to the threshold

used to identify fibrosis from LGE MRI images. We aimed to explore the changes in simulated reentry to the selection of fibrosis threshold and identify simulation output metrics that could be used to create an interpretable and comprehensive understanding of model behavior in subsequent UQ analyses based on realistic ranges of fibrosis values. Using a single patient-specific atrial geometry, we varied the fibrosis threshold and tracked changes in simulated reentrant activity across the model.

2. Methods

2.1. Geometric Model Generation

An LGE-MRI of a patient with a previous ablation was obtained from the University of Utah Hospital database. All data acquisition and procedures were approved by the University of Utah Internal Review Board (IRB). The LGE-MRI images were manually segmented to obtain the left atrial endocardial surface using Corview (The University of Utah, Salt Lake City, United States). Scar and fibrosis were mapped to the endocardial surface from the segmentation, which was then dilated by 1.5 mm to obtain the epicardial surface. Using these surfaces, we generated a tetrahedral mesh with TetGen [7]. The myocardial fiber orientation was then mapped from the human atrial fiber atlas to our meshes using the universal atrial coordinate system [8, 9]. The average edge length of the meshes was 0.644 mm.

2.2. Grid Search of Fibrosis Thresholds

We applied fibrosis and scar thresholding using the image intensity ratio (IIR) based on a range of approaches described in the literature [10–12]. Pixels with an IIR > 1.62 were considered scar; for fibrosis, we selected eight evenly spaced thresholds, ranging from 0.93 to 1.46. These thresholds became the source of variability in the simulations.

2.3. Computational Simulations of AAF

Simulations were performed using the monodomain formulation in openCARP [13] with the Courtemanche ionic model to generate human atrial action potentials [14]. The parameters of the Courtemanche models were adjusted in each tissue region as shown in Table 1. The conductivities of each tissue region were also adjusted to achieve a longitudinal conduction velocity of 0.80 m/s and transverse conduction velocity of 0.40 m/s in the healthy tissue (Table 2) [15].

To induce atrial flutter, we applied a stimulus from nine individual sites. Each stimulus consisted of eight S1 pulses with a cycle length of 600 ms. The S1 pulses were followed by a premature S2 pulse, ranging from 180 to 250 ms after the final S1 pulse. If activity was detected after the S2 pulse (nodes with potential $>$ -40 mV), the simulation was continued for 1.9 s after the S2 beat to let the reentrant activity propagate and either become stable or fade away. Reentrant activity that sustained for the entire 1.9 seconds around the same site was defined as AAF.

Tissue Region	G_{Kr}	G_{Na}	G_{K1}	G_{to}	G_{CaL}
Healthy	1.6	2.0	0.8	0.5	0.3
Fibrosis	1.6	1.2	0.4	0.5	0.15
Scar	1.6	1.2	0.4	0.5	0.15

Table 1. Ionic Model Factors. The Ionic model parameters and the factor they were multiplied by for each region.

Tissue Region	Longitudinal (S/m)	Transverse (S/m)
Healthy	0.3479	0.1606
Fibrosis	0.0627	0.0627
Scar	0.0000	0.0000

Table 2. Conductivity Parameters. The conductivity parameters in each fiber direction for all three regions.

3. Results

3.1. Reentry Duration

The ability to induce flutter across all thresholds and stimulus sites is shown in Figure 1. Reentrant activity occurred following pacing from each stimulus sites. Stimulus site 3 was the only site incapable of inducing AAF. Stimulus sites 4 and 9 resulted in AAF across all fibrosis thresholds. The ability to induce AAF varied based on the fibrosis levels for stimulus sites 1, 2, 5, 6, 7, and 8.

3.2. Activation Maps

The response of simulated activation to threshold selection is illustrated in Figure 2, which shows activation maps for stimulus site 2 across fibrosis thresholds. These activation maps correspond to the reentrant activity plotted in Figure 1. The maps showed three substantially different sites of reentrant activity corresponding to three different fibrosis thresholds. The first site appeared to rotate around a patch of fibrosis on the lower anterior part of the atrium, and was observed at IIR thresholds of 0.93 and 1.01. The next site of reentrant activity was around a large patch of scar on the posterior side of atrium, observed only with a threshold of 1.08. The final site of reentrant activity was around a patch of fibrosis on the roof, which occurred at the thresholds, 1.16, 1.24, 1.31, and 1.39.

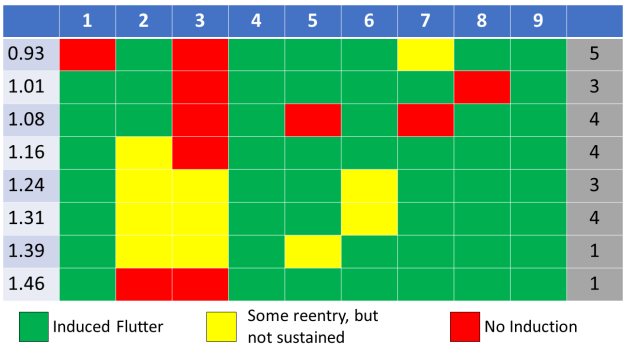

Figure 1. The inducibility at each fibrosis threshold. The rows correspond to the fibrosis threshold, and the columns to the stimulus site. Only durations of > 1.9 ms were considered to be AAF (green). Durations of < 1.9 ms were considered "some reentry" (yellow), whereas duration of 0 were "no induction" (red). The number of unique circuits observed at each threshold is shown in the final column.

4. Discussion

In this study, we simulated atypical atrial flutter using a typical range of fibrosis thresholds in a single patient geometry. Our aims were 1) to explore the sensitivity of simulated reentry to the selection of fibrosis threshold used to create the geometric model of the atria, and 2) to identify simulation output metrics that could be used to create an interpretable and comprehensive understanding of model behavior.

The most notable result was the dramatic changes in reentrant duration and location in response to small changes in the threshold levels of fibrosis, even when pacing occurred from the same site. The ability to sustain flutter also depended on the fibrosis threshold and, less surprisingly, on the pacing site location. Reentry duration and the stability of sustained AAF appeared to be independent of the location of the flutter circuit. Although we observed changes in simulation behavior throughout the range of fibrosis-threshold values, the majority of changes to the duration of reentry occurred within an IIR range of 1.01 to 1.39, a range that captures the values proposed in the literature [10, 11]. The profound variability of the resulting arrhythmias calls for further study using sophisticated UQ approaches to capture what is clearly a nonlinear relationship.

Our second goal remains unresolved, limited by the ability of a single output metric to capture such variability as the path of a reentrant circuit. The duration of each circuit is a possible candidate metric; however, it is not clear what clinical meaning this value has when characterizing a circuit or suggesting possible ablation targets.

This study was limited to a single patient's atrial anatomy and scar pattern; the obvious next step is to expand to more cases. Previous studies have shown other factors besides fibrosis can affect reentry, such as shape, size, and baseline conduction velocities[16]. Each of these parameters introduces another source of uncertainty in parameter selection and another motivation for advanced UQ studies to establish the sensitivity of simulation outputs to these uncertainties.

Acknowledgments

Support for this research came from the Center for Integrative Biomedical Computing (www.sci.utah.edu/cibc), NIH grants P41 GM103545, R24 GM136986, and U24EB029012. NIH/NHLBI grants T32HL007576 (to JAB), and 5F31HL162527 (to EK) and the Nora Eccles Harrison Foundation for Cardiovascular Research.

References

[1] Gucuk Ipek E, Marine J, Yang E, Habibi M, Chrispin J, Spragg D, Berger RD, Calkins H, Nazarian S. Predictors and Incidence of Atrial Flutter After Catheter Ablation of Atrial Fibrillation. The American Journal of Cardiology December 2019;124(11):1690–1696. ISSN 0002-9149.

[2] Balt JC, Klaver MN, Mahmoodi BK, van Dijk VF, Wijffels MCEF, Boersma LVA. High-density versus low-density mapping in ablation of atypical atrial flutter. Journal of Interventional Cardiac Electrophysiology An International Journal of Arrhythmias and Pacing December 2021; 62(3):587–599. ISSN 1572-8595.

[3] Lange M, Kwan E, Dosdall DJ, MacLeod RS, Bunch TJ, Ranjan R. Case report: Personalized computational model guided ablation for left atrial flutter. Frontiers in cardiovascular medicine January 2022;9:893752. ISSN 2297-055X.

[4] Johnstone RH, Chang ETY, Bardenet R, de Boer TP, Gavaghan DJ, Pathmanathan P, Clayton RH, Mirams GR. Uncertainty and variability in models of the cardiac action potential: Can we build trustworthy models? Journal of Molecular and Cellular Cardiology July 2016;96:49–62. ISSN 0022-2828.

[5] Hopman LHGA, Bhagirath P, Mulder MJ, Eggink IN, van Rossum AC, Allaart CP, Götte MJW. Quantification of left atrial fibrosis by 3D late gadolinium-enhanced cardiac magnetic resonance imaging in patients with atrial fibrillation: impact of different analysis methods. European Heart Journal Cardiovascular Imaging November 2021;23(9):1182–1190. ISSN 2047-2404.

[6] Narayan A, Liu Z, Bergquist JA, Charlebois C, Rampersad S, Rupp L, Brooks D, White D, Tate J, MacLeod RS. UncertainSCI: Uncertainty quantification for computational models in biomedicine and bioengineering. Computers in Biology and Medicine January 2023;152:106407.

[7] Si H. TetGen, a Delaunay-Based Quality Tetrahedral Mesh Generator. ACM Trans Math Software February 2015; 41(2):11:1–11:36.

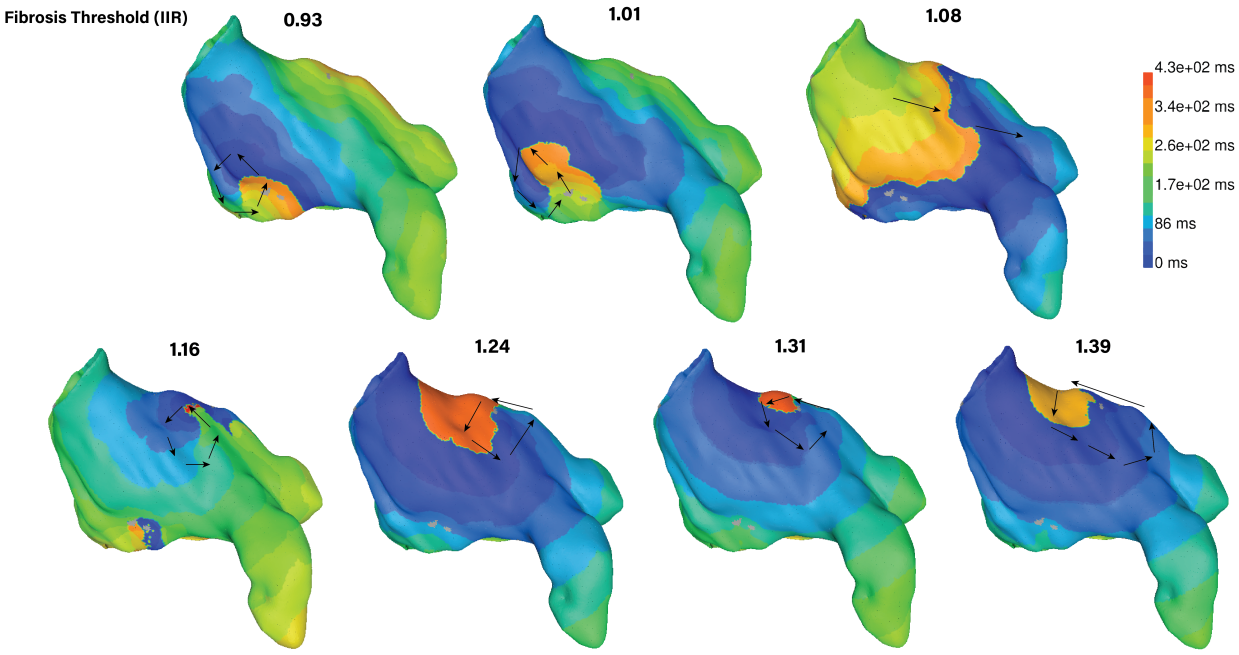

Figure 2. Activation maps. An AP view of one cycle of activation from stimulus site 2 across fibrosis thresholds. Areas in gray represent scar, which does not activate. Arrows indicate the reentrant pathway.

[8] Roney CH, Pashaei A, Meo M, Dubois R, Boyle PM, Trayanova NA, Cochet H, Niederer SA, Vigmond EJ. Universal atrial coordinates applied to visualisation, registration and construction of patient specific meshes. Medical Image Analysis July 2019;55:65–75. ISSN 1361-8415.

[9] Roney CH, Bendikas R, Pashakhanloo F, Corrado C, Vigmond EJ, McVeigh ER, Trayanova NA, Niederer SA. Constructing a Human Atrial Fibre Atlas. Annals of Biomedical Engineering January 2021;49(1):233–250. ISSN 1573-9686.

[10] Khurram IM, Beinart R, Zipunnikov V, Dewire J, Yarmohammadi H, Sasaki T, Spragg DD, Marine JE, Berger RD, Halperin HR, Calkins H, Zimmerman SL, Nazarian S. Magnetic resonance image intensity ratio, a normalized measure to enable interpatient comparability of left atrial fibrosis. Heart Rhythm January 2014;11(1):85–92. ISSN 1547-5271.

[11] Benito EM, Carlosena-Remirez A, Guasch E, Prat-González S, Perea RJ, Figueras R, Borràs R, Andreu D, Arbelo E, Tolosana JM, Bisbal F, Brugada J, Berruezo A, Mont L. Left atrial fibrosis quantification by late gadolinium-enhanced magnetic resonance: a new method to standardize the thresholds for reproducibility. EP Europace August 2017;19(8):1272–1279. ISSN 1099-5129.

[12] Bertelsen L, Alarcón F, Andreasen L, Benito E, Olesen MS, Vejlstrup N, Mont L, Svendsen JH. Verification of threshold for image intensity ratio analyses of late gadolinium enhancement magnetic resonance imaging of left atrial fibrosis in 1.5T scans. The International Journal of Cardiovascular Imaging 2020;36(3):513–520. ISSN 1569-5794.

[13] Plank G, Loewe A, Neic A, Augustin C, Huang YL, Gsell MAF, Karabelas E, Nothstein M, Prassl AJ, Sánchez J, Seemann G, Vigmond EJ. The openCARP simulation environment for cardiac electrophysiology. Computer Methods and Programs in Biomedicine September 2021; 208:106223. ISSN 0169-2607.

[14] Courtemanche M, Ramirez RJ, Nattel S. Ionic mechanisms underlying human atrial action potential properties: insights from a mathematical model. The American Journal of Physiology July 1998;275(1):H301–321. ISSN 0002-9513.

[15] Angel N, Li L, Macleod RS, Marrouche N, Ranjan R, Dosdall DJ. Diverse Fibrosis Architecture and Premature Stimulation Facilitate Initiation of Reentrant Activity Following Chronic Atrial Fibrillation. Journal of Cardiovascular Electrophysiology 2015;26(12):1352–1360. ISSN 1540-8167. eprint: https://onlinelibrary.wiley.com/doi/pdf/10.1111/jce.12773.

[16] Corrado C, Roney CH, Razeghi O, Lemus JAS, et al. Quantifying the impact of shape uncertainty on predicted arrhythmias, 2023.

Address for correspondence:

Ben Orkild
The Nora Eccles Harrison CVRTI
University of Utah
95 S 2000 E
Salt Lake City, UT 84112-5000
ben.orkild@utah.edu